Agricultural and Forest Meteorology 372 (2025) 110692

Contents lists available at ScienceDirect

Agricultural and Forest Meteorology

journal homepage: www.elsevier.com/locate/agrformet

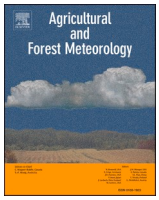

Long-term variations in the ratio of transpiration to evapotranspiration and their drivers in a humid subalpine forest

Yuhao Xiang [a], Genxu Wang [a], Arthur Gessler [b,c], Xiangyang Sun [a], Shan Lin [a], Zishu Tang [a], Shouqin Sun [a], Zhaoyong Hu [a,b,*]

[a] State Key Laboratory of Hydraulics and Mountain River Engineering, College of Water Resource and Hydropower, Sichuan University, 610065, Sichuan, China
[b] Research Unit Forest Dynamics, Swiss Federal Institute for Forest, Snow and Landscape Research WSL, 8903 Birmensdorf, Switzerland
[c] Institute of Terrestrial Ecosystems, ETH Zurich, 8092 Zurich, Switzerland

ARTICLE INFO

Keywords:
Subalpine coniferous forest
Machine learning
Penman-Monteith equation
Water relation

ABSTRACT

Identifying the temporal variations in transpiration (T) and its contribution to evapotranspiration (ET) (T/ET) is of great significance for understanding the mechanisms of ecosystem water distribution and energy partitioning. However, there is a lack of knowledge on the long-term variations in T and ET in high-altitude subalpine regions with low temperature and high humidity. Therefore, the T and ET of a subalpine coniferous forest in Mount Gongga was simulated during the growing season from 2005 to 2021 using three machine learning models and a generalized nonlinear complementary principle model. Results showed that the machine learning models performed better in simulating T than the often-applied Penman-Monteith model. The mean daily and growing season T were 1.18 ± 0.14 mm d^{-1} and 217.60 ± 17.76 mm yr^{-1}, respectively. There was a decreasing trend of T during 2005–2021, with a rate of -2.46 mm yr^{-1} ($P < 0.05$). Variation in T was mainly influenced by net radiation, wind speed, vapor pressure deficit, and relative humidity, and the magnitude of these effects varied at different temporal scales (daily, monthly, and annual). Mean growing season T/ET was 0.46 ± 0.03. There was no significant trend in T/ET before 2016 ($P > 0.05$), but the T/ET significantly decreased thereafter with a rate of 0.01 yr^{-1} ($P < 0.05$). There was no significant difference in T/ET among years with different precipitation at our study site which had always abundant precipitation of >1400 mm. Changes in T/ET were more sensitive to air temperature, and the effect of meteorological factors on T/ET varied at daily, monthly and annual time scales. The decrease in T/ET was primarily due to the continuous increase in temperature in recent years. Our findings indicate that future climate warming will lead to an increase in water resources in subalpine humid regions.

1. Introduction

Evapotranspiration (ET) is a crucial hydrological process in forest ecosystems, serving as the primary pathway for ecosystem water consumption (Schlesinger and Jasechko, 2014; Xu et al., 2022). ET comprises soil evaporation, vegetation transpiration (T), and canopy interception (Jasechko et al., 2013; Xiao et al., 2013). Among the three components of ET, T plays a particularly critical role in forest ecosystems (Wang et al., 2021; Wei et al., 2017). T acts as an essential indicator and component of vegetation water use efficiency, highlighting the importance of this process for maintaining healthy forest ecosystems (Murdiyarso et al., 2015; Wu et al., 2022). Due to the interweaving of plant transpiration and photosynthesis, estimating the changes in T accurately is also crucial in understanding plant growth and carbon cycling (Zhan et al., 2022). The accurate quantification of T and its contribution to ET (T/ET) is also important to understand the global water cycle, guiding ecosystem management, and achieving sustainable water resource use.

Numerous studies have examined the changes in T and ET in response to environmental drivers across various forest ecosystems. Despite this, significant controversy remains regarding the extent to which T contributes to ET (Petrik et al., 2022; Ren et al., 2019). Globally, the T/ET ratio varies widely, ranging from 0.20 to 0.70 (Lian et al., 2018; Schlesinger and Jasechko, 2014). Notably, T/ET values exhibit considerable variation depending on region, vegetation type, and estimation methods. Several studies highlight high contributions of T to ET. For instance, Jasechko et al. (2013) used an isotope tracing method to estimate that T accounts for 80–90 % of ET, making it the largest water

* Corresponding author.
E-mail address: huzy@scu.edu.cn (Z. Hu).

https://doi.org/10.1016/j.agrformet.2025.110692
Received 21 January 2024; Received in revised form 8 June 2025; Accepted 11 June 2025
Available online 17 June 2025

flux from Earth's continents. In contrast, Lian et al. (2018) found a lower global T/ET ratio of 0.62 ± 0.06 by integrating CMIP5 Earth system models (ESMs) with 33 field measurements. Similarly, Zhou et al. (2016) reported annual T/ET ratios ranging from 0.62 to 0.75 for maize and 0.53 to 0.69 for soybean, based on half-hourly flux data from 17 AmeriFlux sites. Cao et al. (2020) reinforced these findings by using the Shuttleworth-Wallace (S-W), Priestly-Taylor Jet Propulsion Laboratory (PT-JPL), and Ecosystem Water Use Efficiency (WUE) models, yielding annual average T/ET values of 0.61 ± 0.14, 0.52 ± 0.12, and 0.59 ± 0.07, respectively. Collectively, these studies indicate that T is a primary component of ET. While these investigations have enhanced our understanding of transpiration's contribution to ET, discrepancies remain regarding T/ET values across different ecosystems. Thus, gathering more ecosystem- and environmental context-specific T/ET data is essential for accurately estimating terrestrial water flux and further elucidating the interactions between terrestrial ecosystems and the atmosphere (Lian et al., 2018; Zhou et al., 2018).

Previous studies have tried to identify the influence of meteorological and biological factors on changes in T/ET, but the conclusions vary depending on the ecological context, environmental conditions and methods. Some studies found that vegetation played a dominant role in the partitioning of ET, suggesting the leaf area index (LAI) as the main driving factor of the spatiotemporal variability in T/ET (Lian et al., 2018; Sun et al., 2020; Zhou et al., 2018). However, the methods applied may overestimate the role of LAI (Lian et al., 2018), and some studies found that the correlation between LAI and T/ET was not statistically significant (Fatichi and Pappas, 2017; Gu et al., 2018). Sun et al. (2020) concluded that the T/ET in humid subalpine ecosystems was mainly controlled by net radiation (R_n) and air temperature (T_{air}) in four different vegetation types, and the influence of these environmental factors on T/ET gradually increased with increasing altitude. Additionally, some studies suggest that T/ET decreased with increasing drought and decreasing precipitation (Paschalis et al., 2018; Schlesinger and Jasechko, 2014), while Ren et al. (2019) found no significant relationship between T/ET and annual precipitation. These studies often focused at a specific time scale, but there might have been differences in the impact meteorological factors on T/ET at different time scales, i.e., daily, monthly, and annual scales (Han et al., 2023). Moreover, previous studies often addressed mostly arid or high temperature regions, with less research conducted in high-humid and low-temperature regions (Ventura et al., 2006; Wu et al., 2022). Therefore, we deem it necessary to study the relationship between T/ET and meteorological factors at different temporal scales and especially in high-humidity and low-temperature subalpine regions.

Compared with other regions, subalpine areas are characterized by a highly variable climate, with low temperatures, strong winds, abundant precipitation, and high humidity, along with distinct seasonal variations (Fan and Lu, 2010). This type of environment is rather unfavorable for plant growth, as T is low and this may ultimately result in lower T/ET (Hou et al., 2023; Tang et al., 2023). The primary soil types in the subalpine ecosystems are alpine gray soil and mountain dark brown soil, which are characterized by thin soil layers, slow weathering, and good drainage. These soil conditions may limit the water uptake capacity of plant roots, thereby constraining T/ET (Tang et al., 2022). Although some studies have been conducted on ecohydrological processes in such regions (Hu et al., 2023, 2018; Sun et al., 2020), it is difficult to obtain generalized results for the temporal variations in T and T/ET due to the complex terrain and lack of long-term continuous monitoring data. Therefore, three machine learning models (Random Forest, Support Vector Regression and Multi-layer Perceptron) and a generalized nonlinear formulation of the complementary principle were established to estimate the long-term (2005–2021) T and ET of a subalpine forest using short-term observational data of T (2017–2018) combined with the long-term meteorological data (2005–2021). The objectives of this study are: (1) to clarify the long-term variations (2005–2021) in T and its contribution to ET in the subalpine humid forest ecosystem, and (2) to elucidate the main controlling factors (temperature, radiation, vapor pressure deficit, wind speed, relative humidity and precipitation) of the variations in T/ET on different temporal scales (daily, monthly, and annual). The findings of this study improve the assessment of climate-driven water fluxes (including temperature, humidity and precipitation effects on T/ET dynamics), providing managers with actionable metrics for water resource management and ecological protection. Furthermore, understanding the trends in T/ET changes is essential for developing adaptive management strategies to address climate change and optimize ecosystem services, while also having a direct impact on regional water cycles (Jasechko et al., 2013).

2. Material and methods

2.1. Site description

The study site Hailuogou is located on the Mount Gongga (29°20′~30°20′ N; 101°30′~102°15′ E). Hailuogou is situated in the subtropical monsoon climate zone and is characterized by a continental monsoon plateau climate. Due to its location on the edge of the Qinghai-Tibet Plateau and its high altitude, some scholars also classify it as a climate of the Qinghai-Tibet Plateau. The area is characterized by distinct wet and dry seasons, with precipitation concentrated from May to October (the wet season). The dry season lasting from November to the following April is characterized by clear weather, large temperature differences between day and night, strong sunlight, low air temperature, and dry air. The study was conducted in a coniferous forest at an altitude of 3000 m asl. (29°33′ N; 101°59′ E). The forest exhibits a mean growing-season leaf area index (LAI) of 3.94 ± 0.32, with minimal interannual variation (Δ_{LAI} = 0.01 between 2017 and 2018), indicating stable canopy conditions. The mean annual air temperature and precipitation of the study site are 4.43 ± 0.54 °C and 1898.40 ± 174.41 mm yr^{-1} (1988–2019) (Wu et al., 2013). This climatic condition promotes significant changes in water dynamics and plant physiological responses, providing favorable conditions for studying the seasonal variations of T and ET. The dominant soil type of the study site is subalpine gray soil, with some mountainous dark brown soil (Tang et al., 2022). The parent material of the soil underwent slow weathering, resulting in a long soil formation time. As a result, the soil layers were generally thin and predominantly composed of weathered small gravel and the soil pH ranges from 4.00 to 5.00, which may restrict water absorption and root development in plants, thus affecting the variations of T and ET (Carminati et al., 2017). The height of the *Abies fabri* dominating the ecosystem examined ranges from 15 to 40 m and the diameter at breast height is between 0.40 to 0.80 m (Wang et al., 2017; Zhou, 2013).

2.2. Meteorological observation

Meteorological sensors were installed at 30 m on a meteorological observation tower. The meteorological observation data was collected at 30-min frequency. To facilitate long-term simulation and analysis, these half-hour data were processed and converted into daily scale data. The experiment monitored meteorological variables, such as precipitation (P_{re}, mm), T_{air} (°C), relative humidity (RH, %), wind speed (Ws, m s^{-1}), etc. Soil temperature (T_{soil}, °C) probes were installed at 5 cm, 10 cm, 20 cm and 40 cm soil depth. The meteorological station was located 10 m away from the study site. The upward longwave radiation (R_{ul}), upward shortwave radiation (R_{us}), downward longwave radiation (R_{dl}) and downward shortwave radiation (R_{ds}) were measured with an NR01 sensor (Hukseflux, Netherlands) at 30 m. Net radiation (R_n) was calculated as:

$$R_n = (R_{dl} + R_{ds}) - (R_{ul} + R_{us}) \quad (1)$$

The vapor pressure deficit (VPD, kPa) was calculated from T_{air} and RH using the following formula (Allen et al., 1998):

$$VPD = (1 - RH)\left(0.611 \times \frac{17.502T_a}{e^{T_{air}+240.97}}\right) \quad (2)$$

2.3. Transpiration measurement

Transpiration drives plants to absorb water through their roots and transport it through the trunk to the leaves, forming sap flow. Measuring sap flow allows for real-time understanding of water transport within the plant and its water utilization status (Granier et al., 1996). Sap flow densities of the tree stem were measured using thermal dissipation probes (TDP-30, Dynamax, USA) installed at breast height (1.30 m) on each of the 12 sample trees. The sap flow density of each tree was calculated following Granier et al. (1996) based on the temperature difference between heated and reference sensors:

$$V_s = 0.0119 \times \left(\frac{\Delta T_m - \Delta T}{\Delta T}\right)^{1.231} \quad (3)$$

where V_s is the sap flow density of the sapwood of the tree stem (cm s^{-1}); ΔT_m is the maximum temperature difference between the probes within 24 h (°C); ΔT is the instantaneous temperature difference between the two probes (°C), which is calculated by dividing the voltage difference outputted by the TDP probes by an empirical constant of 0.04.

Then transpiration rate for single trees (T_s, g h^{-1}) was calculated:

$$T_s = V_s * S * 3600 \quad (4)$$

where S (cm^2) is the sapwood area of the selected tree.

After calculating the sap flow rate of individual trees, the 12 sample trees were classified into three size classes based on diameter frequency distribution, and stand transpiration was computed using the formula from Hatton et al. (1990):

$$T = 10 * \sum\left(\frac{T_{si}}{S_a}\right) \quad (5)$$

where T (mm h^{-1}) is the total transpiration of the stand at the stand level; T_{si} (g h^{-1}) is the transpiration rate of trees of diameter class i; S_a is the area of the plot (cm^2). This approach enables accurate assessment of the forest's water demand by accounting for variations in tree size and stand structure (Jiménez-Rodríguez et al., 2024).

2.4. Models for ET and T simulation

2.4.1. ET simulation

ET was simulated by a generalized nonlinear formulation of the complementary principle (Brutsaert, 2015):

$$ET = \left(\frac{ET_{po}}{ET_{pa}}\right)^2 (2ET_{pa} - ET_{po}) \quad (6)$$

ET_{pa} is the apparent potential evapotranspiration, defined as the evapotranspiration from a small wet area under a drying environment which is the same as that for actual evapotranspiration. ET_{po} is the potential evapotranspiration, defined as the maximum evapotranspiration under conditions with an abundant water source. ET_{pa} and ET_{po} can be estimated using the Penman equation (Penman, 1948) and the Priestley and Taylor equation (Priestley and Taylor, 1972), respectively:

$$ET_{pa} = \frac{\Delta}{\Delta + \gamma} Q_{ne} + \frac{\gamma}{\Delta + \gamma} f_e(u_1)(e_2^* - e_2) \quad (7)$$

$$ET_{po} = \alpha_e \frac{\Delta}{\Delta + \gamma} Q_{ne} \quad (8)$$

α_e is not quite the Priestley-Taylor parameter, but is merely a weak analogue of it; Δ is the slope of the saturation vapor pressure curve relative to temperature (kPa $°C^{-1}$); γ is the psychrometric constant (kPa $°C^{-1}$); Q_{ne} is the available energy in water depth (mm), defined as $Q_{ne}=(R_n\text{-}G)/\rho\lambda$; G is the soil heat flux (W m^{-2}); λ is the latent heat of vaporization (kJ kg^{-1}); ρ is the density of water (kg m^{-3}); u_1 is the mean wind speed at a height z_1 above the surface (m s^{-1}); f_e (u_1) is a wind function; e_2^* and e_2 are the saturation vapor pressure and the actual vapor pressure (kPa), respectively, at a height z_2 above the surface. Because the daily average atmospheric stability is considered neutral (Cheng and Brutsaert, 2005), the wind function is estimated by the following equation:

$$f_e(u_1) = \frac{0.622k^2 u_1}{R_d T_a \ln[(z_2 - d)/z_{0v}] In[(z_1 - d)/z_0]} \quad (9)$$

where k is the von Karman constant ($k = 0.40$); R_d is the specific gas constant for dry air (0.29 kJ kg^{-1} K^{-1}); T_a is the mean air temperature (K); z_0 is the momentum roughness (m); z_{ov} is the scalar roughness (m); d is the displacement height of the zero plane (m).

At our study site with a coniferous forest, the values of α_e, z_0, z_{ov} and d were 1.10, 3.50 m, 0.35 m and 18.76 m, respectively. Daily ET simulation using the generalized nonlinear formulation of the complementary principle with these parameters for the study area has been validated; more details can be found in Hu et al. (2018).

2.4.2. T simulation

With the rapid advancement of artificial intelligence and machine learning technologies in recent years, machine learning models have been extensively applied to simulate T (Sperling et al., 2023). In this study, we employed T from sap flow measurements using Granier thermal dissipation probes as the dependent variable, with T_{air}, T_{soil}, R_n, VPD, Ws, and RH serving as independent variables. Three representative machine learning algorithms were implemented: Random Forest (RF), Support Vector Regression (SVR), and Multilayer Perceptron (MLP). These models effectively captured the complex nonlinear relationships between environmental drivers and transpiration, demonstrating satisfactory simulation performance (Ellsasser et al., 2020; Kassanuk and Phasinam, 2022).

(1) Random Forest (RF)

Random Forest is an ensemble method that aggregates predictions from multiple decision trees to improve accuracy and reduce overfitting (Breiman, 2001). We implemented RF regression with 500 decision trees (max depth=10 nodes, MSE splitting criterion).

(2) Multi-Layer Perceptron (MLP)

The Multilayer Perceptron is a feedforward neural network that learns hierarchical representations through multiple interconnected layers (Chen et al., 2013). The model progressively extracts features through nonlinear transformations across layers, ultimately achieving end-to-end pattern recognition and prediction tasks via fully connected layers (Benardos and Vosniakos, 2007). Our architecture consists of 1 input layer, 2 hidden layers (130 and 70 neurons, respectively), and 1 output layer. The hidden layers use ReLU activation, and the model is trained using the Adam optimizer with a learning rate of 0.001.

(3) Support Vector Regression (SVR)

Support Vector Regression is a supervised learning algorithm that constructs an optimal hyperplane in high-dimensional space to approximate nonlinear relationships while tolerating specified deviations (ε-tube) (Chang and Lin, 2011). The model's robustness stems from its dual formulation that applies kernel tricks for implicit feature transformation and incorporates Vapnik's ε-insensitive loss function, effectively balancing model complexity with generalization performance (Cortes and Vapnik, 1995). Our implementation utilizes a radial

basis function (RBF) kernel (γ=0.10) with ε=0.01 tolerance and C = 1.00 regularization parameter, where the hyperparameters were determined through exhaustive grid search.

(4) Penman-Monteith (PM) equation

The Penman-Monteith equation is based on the theory of water vapor diffusion and energy balance, and comprehensively considers the physiological and aerodynamic factors of plants. It is widely used to estimate T and has become a standard method in ecohydrology, agricultural water management, and plant physiological studies (Penman, 1948; Monteith, 1965; Petrik et al., 2022). The formula is as follows:

$$T = \frac{\Delta R_n + \alpha\rho^* C_p \frac{e_2^* - e_2}{r_a}}{\lambda\Delta + \lambda\gamma\left(1 + \frac{r_c}{r_a}\right)} \tag{10}$$

where α is the time scale factor and is taken as 86,400; ρ^* is the atmospheric density (kg m^{-3}); C_p is specific heat capacity of air (J kg^{-1} K^{-1}); r_c is the canopy resistance (s m^{-1}); r_a is the aerodynamic resistance (s m^{-1}), which was calculated using the following expression (Allen et al., 1989; Loescher et al., 2005):

$$r_a = 4.72\frac{ln^2\left(\frac{Z-d}{Z_0}\right)}{1 + 0.54u_1} \tag{11}$$

where Z is the observation height for wind speed; Z_0 is the roughness length, taken as 0.1 times the average tree height.

In PM equation, all parameters except for the canopy resistance r_c can be accurately measured using instruments. r_c is determined by the degree of stomatal closure, which is primarily influenced by meteorological factors (Bailey et al., 1993). In this study, we use an empirical formula reverse calculation method to estimate r_c. Specifically, r_c was estimated by measuring all parameters in the PM equation, and constructing a linear regression model between r_c and meteorological factors (VPD, RH, T_{air}) to predict r_c during the growing season.

2.5. Models performance criteria

The effectiveness of forecasting models was assessed by several statistical metrics, i.e., Root Mean Squared Error (RMSE), Mean Absolute Error (MAE), Mean Square Error (MSE), and Coefficient of Determination (R^2). RMSE reflects the average magnitude of the prediction errors, and its sensitivity to larger errors helps highlight significant discrepancies in the model's predictions. MAE provides a straightforward measure of the average errors, giving equal weight to all deviations and therefore offering an intuitive understanding of the model's overall prediction accuracy. MSE quantifies the average of the squares of the errors, emphasizing larger discrepancies and thus allowing for a clear identification of areas where the model performs poorly. R^2 indicates the proportion of variance in the dependent variable that is predictable from the independent variables, aiding in assessing how well the model fits the data and its explanatory power. These metrics were calculated as follows:

$$\mathrm{RMSE} = \sqrt{\frac{1}{n}\sum_{i=1}^{n}(T_s - T)^2} \tag{12}$$

$$\mathrm{MSE} = \frac{1}{n}\sum_{i=1}^{n}(T_s - T)^2 \tag{13}$$

$$\mathrm{MAE} = \frac{1}{n}\sum_{i=1}^{n}|T_s - T| \tag{14}$$

$$R^2 = 1 - \frac{\sum_{i=1}^{n}(T_s - T)^2}{\sum_{i=1}^{n}(\overline{T} - T)^2} \tag{15}$$

where T_s is the simulated value of daily transpiration (mm d^{-1}); T is the measured value of daily transpiration (mm d^{-1}); $\overline{T}$ is the measured average value of daily transpiration (mm d^{-1}); n is the number of days of transpiration simulation.

2.6. Precipitation classification

Years with different precipitation patterns may have different impacts on regional water resource supply, plant growth, and ecosystem functioning (Wu et al., 2022). Therefore, in this study, we distinguished "precipitation years" to assess whether differences in precipitation among years would affect T/ET. The precipitation years were classified using a precipitation departure method (Gocic et al., 2016; Pnevmatikos and Katsoulis, 2006). The variability index of precipitation (D_i) was calculated as:

$$D_i = \frac{(P_i - \overline{P})}{SD} \tag{16}$$

where $D_i$is the variability index of precipitation in year i; P_i is the annual precipitation in the year i; $\overline{P}$ is the multiyear mean annual precipitation; SD is the standard deviation of the annual precipitation series. Basing on the D values, precipitation years can be classified as normal year ($0.5 > D > -0.5$), wet year ($D > 0.5$), and dry year ($D < -0.5$).

2.7. Statistical analysis

Three machine learning models (RF, SVR and MLP) were built using daily T and meteorological data from the growing seasons 2017–2018. The training and test datasets were randomly split in a ratio of 7:3. The machine learning models were then used to simulate T for the periods 2005–2016 and 2019–2021, using the meteorological data during these periods. ET was calculated using the formula described in section 2.3.1 (Eq. 6–9), utilizing meteorological data from the period 2005 to 2021.

To compare with the machine learning models, the PM equation was applied with data from the 2017 to 2018 growing seasons, using the same driving factors (R_n, VPD, RH, Ws and T_{air}) as for the machine learning models.

The Mann-Kendall (MK) test was used to analyze the presence of changes in T, ET, and T/ET as well as the direction of change. UF and UB were statistical variables for the MK test. If the UF value was greater than zero, it indicated an upward trend in the sequence; if smaller than zero, it indicated a downward trend. If the UF line was within the confidence lines, it indicated that the change in the curve trend was not significant. When it exceeded the confidence lines, it indicated a significant upward or downward trend. If the UF and UB lines intersected within the confidence lines, the time corresponding to the intersection point was the start time of the change. The Theil-Sen method was used to quantify the magnitude and determine the significance of the trends (Theil, 1950).

The Pearson correlation analysis method was used to analyze the relationship between T, T/ET, and meteorological factors at different time scales. Stepwise linear regression was used to fit regressions between T/ET and meteorological factors at different time scales.

3. Results

3.1. Meteorological data

Mean annual P_{re} (Fig. 1b) and T_{air} (Fig. 1g) at the study site were 1795.70 ± 204.11 mm yr^{-1} and 4.43 ± 0.54 °C, respectively. The interannual coefficient of variation (CV) for P_{re} and T_{air} were 11.37 % and 7.52 %, respectively. From the precipitation classification analysis

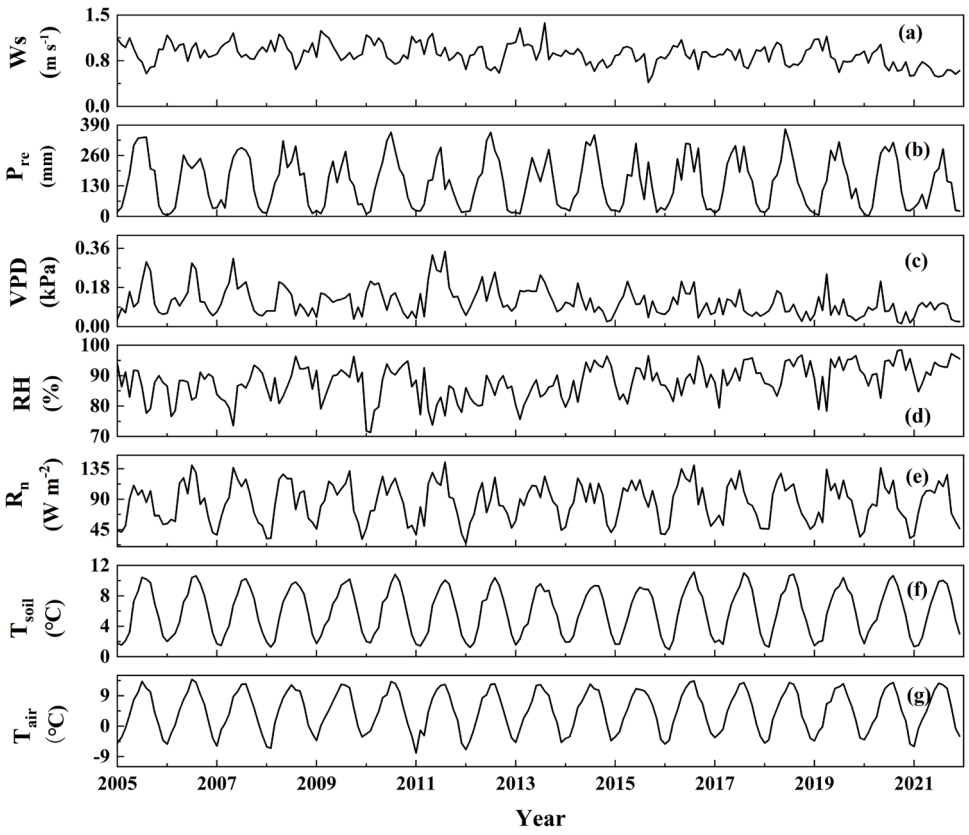

Fig. 1. Monthly variations in (a) wind speed (Ws, m s^{-1}), (b) precipitation (P_{re}, mm), (c) vapor pressure deficit (VPD, kPa), (d) relative humidity (RH, %), (e) net radiation (R_n, W m^{-2}), (f) soil temperature (T_{soil}, °C), and (g) air temperature (T_{air}, °C) of the study site during 2005–2021.

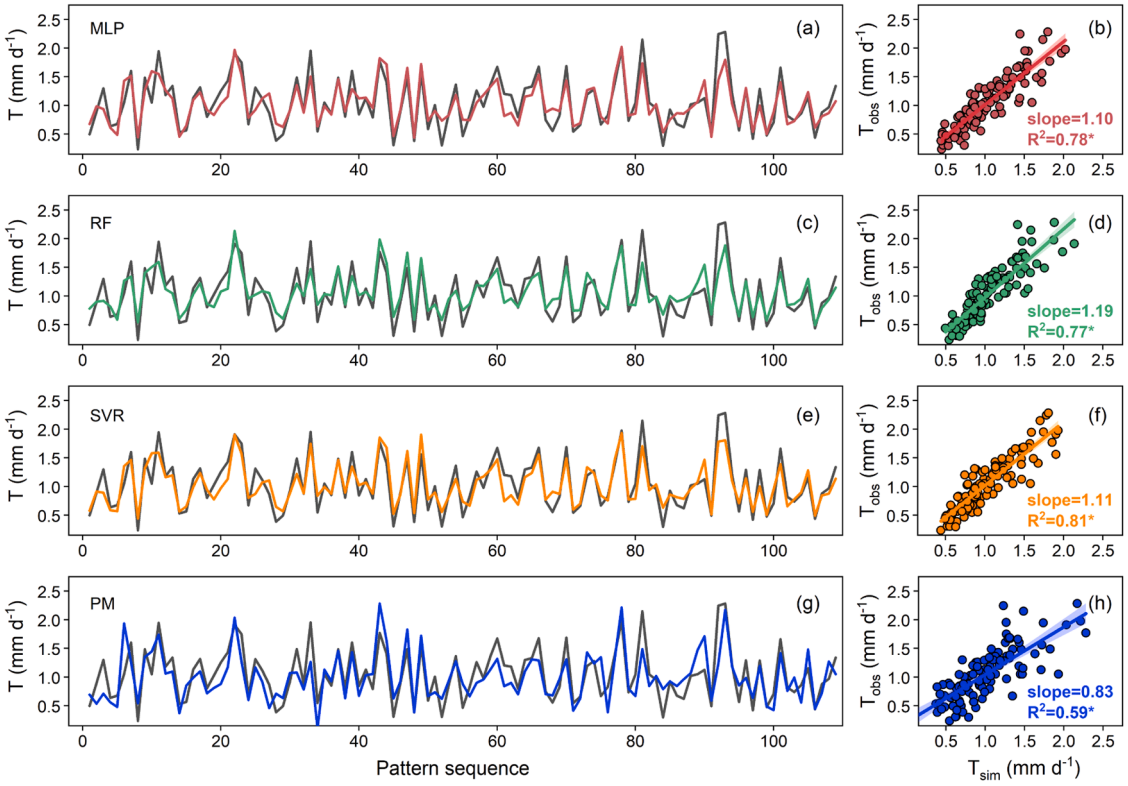

Fig. 2. Comparisons between simulated and observed transpiration (T, mm d^{-1}) using (a and b) Multi-Layer Perceptron (MLP), (c and d) Random Forest (RF), (e and f) Support Vector Regression (SVR) and (g and h) Penman-Monteith (PM) equation. Pattern sequence is a randomly shuffled time sequence.

for the period from 2005 to 2021, the years 2005, 2007, 2008, 2010, and 2018 were defined as wet years; 2009, 2011, 2015, and 2021 were dry years; 2006, 2012, 2013, 2014, 2016, 2017, 2019, and 2020 were normal years. The multi-year mean of Ws was 0.76 ± 0.09 m s^{-1} and the CV was 20.00 % (Fig. 1a). VPD roughly exhibited a bimodal curve on an annual scale, with occasional fluctuations in some years, and the annual mean was 0.11 ± 0.03 kPa. The curve for R_n exhibited bimodal annual patterns and was clearly related to T_{air} and T_{soil}. The RH in the study site was relatively high, with a multi-year mean value of around 90.00 %, with an interannual CV of 6.40 %.

3.2. Performance of the machine learning models in simulating T

All three machine learning models showed good performance in simulating T, with SVR showing the best performance (Fig. 2 and Table S1). The test set R^2, RMSE, MSE and MAE for the SVR were 0.81, 0.20 mm d^{-1}, 0.04 (mm d^{-1})^2 and 0.16 mm d^{-1}, respectively (Fig. 2f). The MLP was the second-best performing model with a test set R^2 of 0.78, RMSE of 0.22 mm d^{-1}, MSE of 0.05 (mm d^{-1})^2 and MAE of 0.17 mm d^{-1} (Fig. 2b). The RF model performed slightly worse than the other two models, with a test set R^2 of 0.77, RMSE of 0.23 mm d^{-1}, MSE of 0.05 (mm d^{-1})^2 and MAE of 0.18 mm d^{-1} (Fig. 2d). The R^2, RMSE, MSE, and MAE values for T simulated by the PM equation were 0.59, 0.30 mm d^{-1}, 0.09 (mm d^{-1})^2, and 0.24 mm d^{-1}, respectively (Fig. 2h), indicating its worse performance compared to the machine learning models. The SVR model incorporates a regularization term, which effectively controls model complexity and helps prevent overfitting. This characteristic enables SVR to perform robustly, particularly in datasets with high noise levels. Additionally, when working with relatively small datasets, SVR tends to outperform other models, such as RF and MLP, which usually require larger datasets to realize their advantages (Arrieta et al., 2020). The results obtained from the three machine learning models were similar, with the same areas of underestimation of extreme values. In this study, the mean values of the results from the three machine learning models were considered as the final simulation results for T.

3.3. Long-term variation in ET, T and T/ET during the growing season

The mean daily variations in ET and T during the growing season were obtained by averaging the multi-year ET and T data of the subalpine coniferous forest (Fig. 3). During the studied period, the mean daily ET was 2.55 ± 0.49 mm d^{-1}, ranging from 1.36 to 3.84 mm d^{-1}. At the beginning of the growing season, ET was around 3.00 mm d^{-1} and decreased from mid-May to approximately 2.50 mm d^{-1} in June. ET increased again from July and reached its peak in August at 3.84 mm d^{-1}. After that, ET continuously decreased to the minimum of 1.36 mm d^{-1} until the end of the growing season. The fluctuation of T showed a similar pattern to that of the ET but with smaller magnitude of the variation. Daily T varied from 0.90 to 1.53 mm d^{-1}, with a mean value of 1.18 ± 0.14 mm d^{-1} during 2005–2021. Mean daily T/ET was 0.47 ± 0.06. During the early growing season (May to June), T/ET showed an opposite trend to that of the ET, fluctuating at around 0.48. T/ET slightly decreased to around 0.42 during the mid-growing season (July to August) and significantly increased towards the late growing season (September to October), with a T/ET of approximately 0.60 in October.

The monthly ET of the subalpine coniferous forest during the growing season from 2005 to 2021 varied from a minimum of 42.76 mm $month^{-1}$ to a maximum of 115.79 mm $month^{-1}$, with an overall mean value of 78.24 ± 16.56 mm $month^{-1}$. The monthly ET showed a significant correlation with the T_{air} ($P < 0.05$), except for the abnormal decrease in June (76.70 ± 10.18 mm $month^{-1}$, 16.33 % of the total growing season ET). The mean ET in August (Fig. 4) was the highest (89.17 ± 16.00 mm $month^{-1}$), accounting for 18.99 % of the total growing season ET. The average ET in September and October declined significantly as the T_{air} dropped and ET reach its lowest value of 57.41 ± 10.2 mm $month^{-1}$ in October, accounting for 12.22 % of the total growing season.

The monthly T of the subalpine coniferous forest during the growing season from 2005 to 2021 exhibited a trend similar to that of the ET, but with smaller magnitude of change and its overall trend was relatively stable, varying from 22.97 to 47.73 mm $month^{-1}$, with a mean value of 36.26 ± 5.57 mm $month^{-1}$. The monthly mean T in May was the highest, amounting to 41.20 ± 3.25 mm $month^{-1}$ and accounting for 18.94 % of the total growing season T. As ET, T also showed a decrease in June (36.10 ± 3.87 mm $month^{-1}$) the month, which made up 16.59 % of the total growing season T. Similar as for ET, the monthly mean T value gradually decreased during the late growing season, reaching its lowest value in October (32.28 ± 3.64 mm $month^{-1}$, 14.84 % of the total growing season). The monthly mean T/ET showed an opposite trend to that of ET. T/ET was highest in October (0.57 ± 0.07), while the mean T/ET values in August (0.42 ± 0.06) were the lowest. It was observed that months with high T/ET values tend to have low ET values and that, thus, the stronger variability of ET compared to T during the growing season strongly drove T/ET patterns.

The mean growing season ET of the subalpine coniferous forest was 469.46 ± 30.88 mm yr^{-1}, with the minimum (417.39 mm yr^{-1}) and maximum (532.49 mm yr^{-1}) values occurring in 2012 and 2016, respectively (Fig. 2). The interannual CV for ET was 6.58 %. There were no significant changes in growing season ET ($P = 0.66$) during the study period (2005–2021). The mean growing season T of the subalpine coniferous forest was 217.58 ± 17.76 mm yr^{-1}. The minimum T value occurred in 2020 (192.42 mm yr^{-1}), and the maximum T value in 2011 (250.29 mm yr^{-1}). T exhibited a non-significant downward trend between 2008 and 2016, followed by a significant downward trend

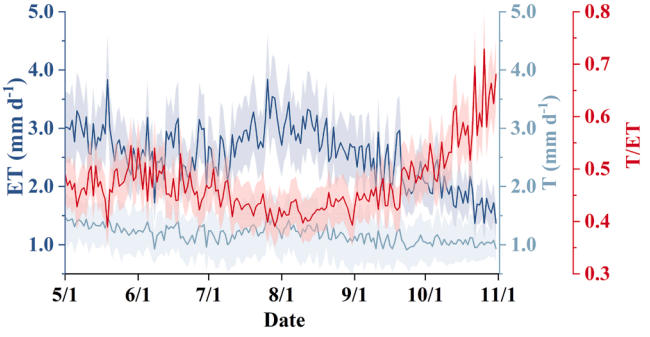

Fig. 3. Mean daily variations in evapotranspiration (ET, mm d^{-1}), transpiration (T, mm d^{-1}), and the ratio of transpiration to evapotranspiration (T/ET) during 2005–2021. Error bars indicate the standard deviation of daily T, ET and T/ET of the years 2005–2021.

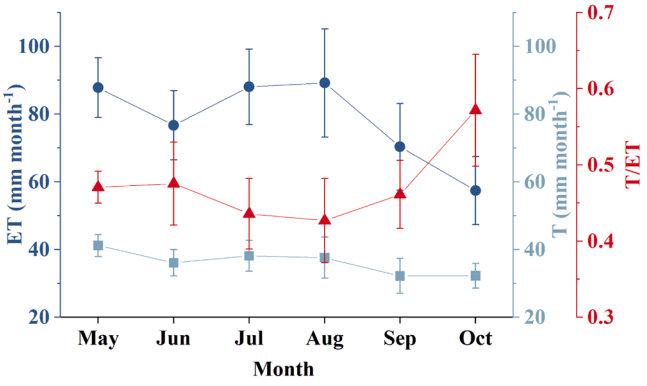

Fig. 4. Mean monthly variations in evapotranspiration (ET, mm $month^{-1}$), transpiration (T mm $month^{-1}$), and the ratio of transpiration to evapotranspiration (T/ET) during 2005–2021. Error bars were the standard deviation of monthly T, ET and T/ET of the years 2005–2021.

between 2017 and 2021, with a sudden change occurring in 2016 (Fig. 6). The overall annual change rate of T was significant ($P < 0.01$) and amounted to −2.46 mm yr^{-2} from 2005 to 2021. The annual T/ET during the growing season of the subalpine coniferous forest ranged from 0.42 to 0.53 and mean annual T/ET was 0.46 ± 0.03. There was no significant trend for T/ET before 2016, while T/ET significantly declined after 2017 with a rate of 0.005 yr^{-1} (Figs. 5 and 6). The median values of monthly T during the growing season for wet, normal, and dry years were 36.32 mm $month^{-1}$, 35.92 mm $month^{-1}$, and 36.84 mm $month^{-1}$, respectively, and there was no significant difference of monthly T among different precipitation years ($P = 0.73$) (Fig. 7a). Similarly, there were no significant differences observed in monthly ET ($P = 0.63$) and T/ET ($P = 0.76$) among the three types of precipitation years (Fig. 7b and c)

3.4. Driving factors of T during the growing season at different time scales

T exhibited significant scale-dependent correlations with meteorological factors (Table 1). At the daily scale, R_n showed the strongest correlation with T, followed by VPD. As the temporal scale expanded to monthly, the dominant effect of R_n weakened, while P_{re} no longer showed significant correlation ($P > 0.05$). At annual scale, VPD became the most critical factor affecting T with significantly enhanced correlation, whereas influence from R_n substantially decreased ($r = 0.37$). RH maintained strong negative correlations with T across all temporal scales ($P < 0.01$), and Ws consistently showed positive correlations ($P < 0.01$). In contrast, T_{soil} had no significant effects, and T_{air} only showed significant positive correlations at the daily and monthly scales ($P < 0.01$). These patterns reveal the multi-scale characteristics of T's response to meteorological factors.

3.5. Driving factors of T/ET during the growing season at different time scales

At the daily scale, there was a significant negative correlation between T/ET and meteorological factors including VPD, T_{air}, T_{soil}, Ws, and R_n ($P<0.05$) (Fig. 8). T/ET exhibited a distinct positive correlation with RH ($P<0.05$), whereas the relationship between T/ET and P_{re} was not evident ($P = 0.17$). R_n was the best explanatory variable for T/ET with an R^2 value of 0.40, followed by T_{air} with an R^2 value of 0.31. Meteorological factors such as Ws, VPD, and P_{re} showed small explanatory power for T/ET with R^2 values <0.10. The stepwise regression analysis of T/ET and meteorological factors resulted in $T/ET = 0.78 - 0.003R_n - 0.024T_{soil} + 0.784VPD - 0.013T_{air} + 0.13Ws - 0.001P_{re} + 0.003\ RH$, which can explain 60.21 % of the daily variation in T/ET of the subalpine coniferous forest. At the daily scale we see some values of T/ET >1 especially at low R_n and high RH (low VPD). This is because

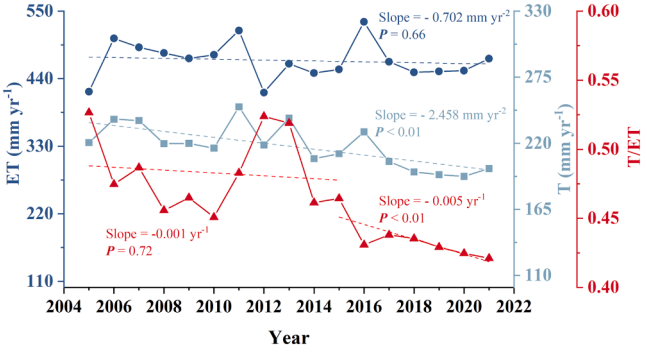

Fig. 5. Annual variations in evapotranspiration (ET, mm yr^{-1}), transpiration (T, mm yr^{-1}), and the ratio of transpiration to evapotranspiration (T/ET). The dashed line in the graph represents the slope curve calculated by the Theil-Sen method.

under these conditions, the estimated ET is often very small (less than T), which indicates larger uncertainty in the estimation of T or ET or both under these conditions.

At the monthly scale, there was a significant negative correlation between T/ET and meteorological factors including T_{air}, T_{soil}, R_n, and P_{re} (Fig. 9). However, the correlations between T/ET and VPD, Ws, and RH were not significant ($P > 0.05$). T_{air} had the best explanatory rate for T/ET and could explain 53.30 % of the variation in T/ET, followed by R_n with an R^2 value of 0.40 and T_{soil} with an R^2 value of 0.33. P_{re} could explain 12.70 % of the variation in T/ET. The stepwise regression analysis of T/ET and meteorological factors at the monthly time scale resulted in $T/ET = 1.340 - 0.009T_{air} - 0.003R_n - 0.006RH + 0.104Ws$, which explained 83.62 % of the monthly variation in T/ET. These findings are consistent with the feature importance and SHAP analysis results presented in Appendix Fig. S2.

At the annual scale, there was a significant negative correlation between T/ET and meteorological factors such as T_{air}, T_{soil}, VPD and RH, while there was a significant positive correlation between T/ET and VPD (Fig. 10). The relationship between R_n and T/ET was no longer significant. Furthermore, RH had the strongest explanatory power for T/ET, explaining 56.00 % of its variation, followed by VPD, which could explain 53.30 % of the variation in T/ET. The explanatory rate of T_{air} for T/ET was lower (32.60 %) than at the monthly scale. By performing stepwise regression analysis of T/ET with meteorological factors at annual time scale, the equation $T/ET = 1.621 - 0.010RH + 0.004R_n$ was obtained, which explained 77.84 % of the annual variation in T/ET.

4. Discussion

4.1. Machine learning models compared with a traditional model in T simulation

The machine learning models simulated T more accurately than the traditional PM model, which is consistent with previous studies (Ellsasser et al., 2020; Kassanuk and Phasinam, 2022). Ellsasser et al. (2020) and Kassanuk and Phasinam (2022) applied classical statistical methods and machine learning models to calculate T and found that machine learning methods have tremendous potential in ecological applications. Machine learning models have a greater ability to identify underlying patterns and regularities within data compared to traditional models and can extract useful features from different data types and integrate and optimize them within the model. Moreover, they are capable of adaptively learning and progressively improving their models (Allawi et al., 2023; Liang et al., 2023). In addition, as the volume and complexity of data increases, they can improve model accuracy and generalization (Schmidhuber, 2015). Furthermore, machine learning models are capable of effectively handling complex non-linear relationships (Jordan and Mitchell, 2015; Lecun et al., 2015). Compared with machine learning models, traditional models still have some advantages. Traditional models typically do not require complex algorithms or large volumes of data sets, making them easier to implement. Moreover, traditional models are typically designed based on specific problems and situations, and have stronger interpretability (Dong et al., 2021). Therefore, to improve the accuracy of the simulations and to make the models interpretable, we should try to combine machine learning or deep learning with traditional models that include mathematical representations of physiological and ecological processes.

4.2. Driving factors for the temporal variations of T during the growing season

In the present study, the average daily T was 1.18 ± 0.14 mm d^{-1} and the multi-year mean T for the growing season was 217.58 ± 17.76 mm yr^{-1}, which was higher than values found in previous studies. Xu et al. (2022) reported a daily average T of 0.60 mm d^{-1} during May to September in a *Larix gmelinii* forest in northern China, while Wang et al.

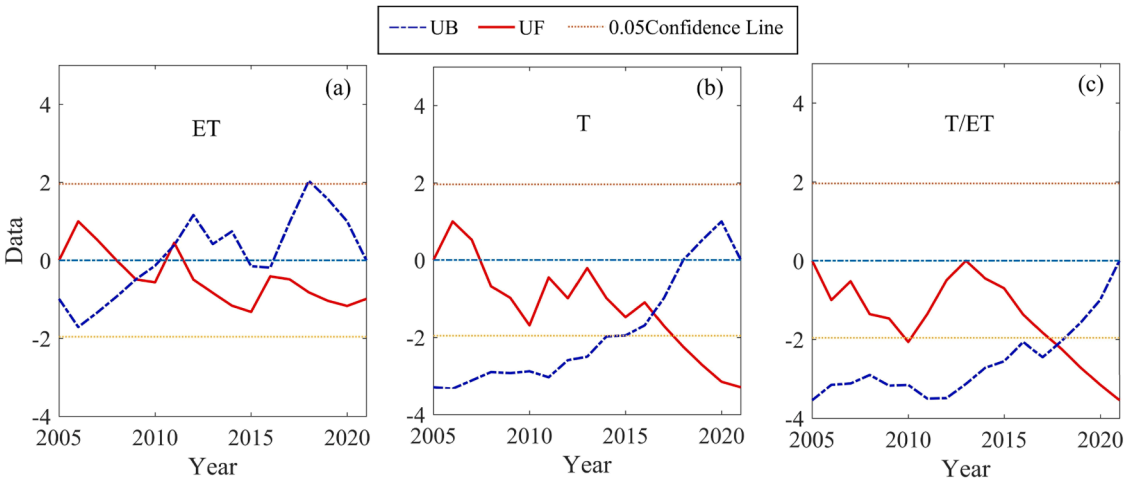

Fig. 6. Annual Mann-Kendall (MK) test for (a) evapotranspiration (ET, mm yr^{-1}), (b) transpiration (T, mm yr^{-1}), and (c) the ratio of transpiration to evapotranspiration (T/ET). UF and UB represent the forward and backward sequences of the Mann-Kendall test statistic, respectively. The intersection points between UF and UB curves indicate potential trend turning points.

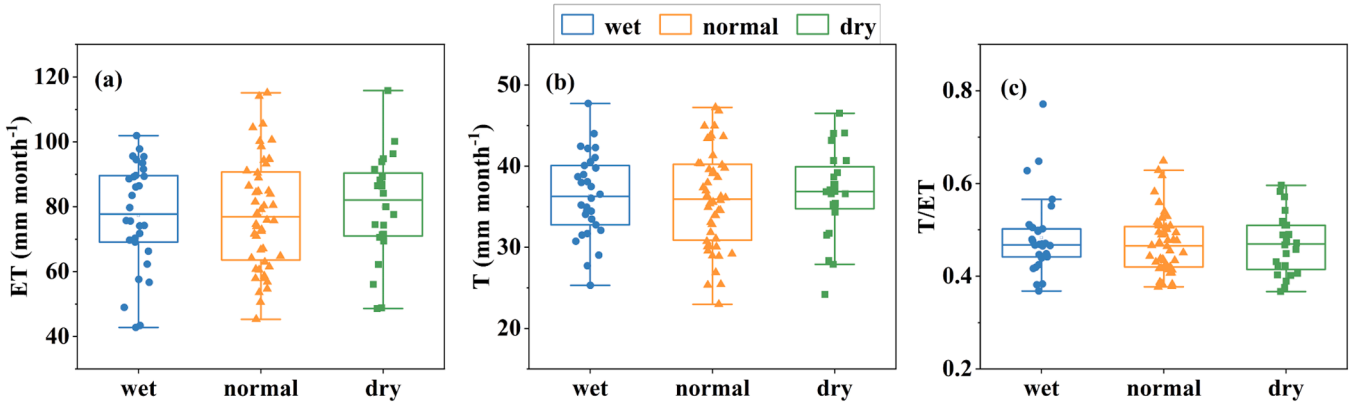

Fig. 7. Mean monthly variations in (a) evapotranspiration (ET, mm $month^{-1}$), (b) transpiration (T, mm $month^{-1}$) and (c) the ratio of transpiration to evapotranspiration (T/ET) for wet (blue), normal (orange) and dry (green) years. The upper and lower edges of the box are the upper (75 %) and lower quartiles (25 %), respectively. The solid line in the box is the median value.

Table 1
The correlation coefficients between transpiration (T, mm) and vapor pressure deficit (VPD, kPa), air temperature (T_{air}, °C), soil temperature (T_{soil}, °C), wind speed (Ws, m s^{-1}), net radiation (R_n, W m^{-2}), relative humidity (RH, %) and precipitation (P_{re}, mm) at daily, monthly and annual scales.

	VPD	T_{air}	T_{soil}	Ws	R_n	RH	P_{re}
Daily	0.81**	0.38**	−0.03	0.77**	0.91**	−0.78**	−0.32**
Monthly	0.83**	0.31**	−0.04	0.75**	0.85**	−0.81**	−0.05
Annual	0.92**	−0.15	−0.35	0.69**	0.37	−0.90**	−0.06

**Indicates significant correlation at level 0.01 (double-tailed).

(2021) found daily average T of 0.70 mm d^{-1} (ranging from 0.02 to 1.55 mm d^{-1}) in coniferous forests during the 2018 growing season. The discrepancies among different studies could be due to differences in tree species, stand density and varying climatic conditions. Climatic conditions directly affect the water demand and T of forests. For example, in arid or semi-arid regions, forests may develop more efficient water use strategies to adapt to the scarcity of water resources. Conversely, in humid areas, trees may prioritize rapid growth and high transpiration rates to take advantage of the abundant water resources (Jump et al., 2017). Stand density also influences the water use strategies of forests. In high-density stands, competition among trees may lead to a decline in the individual trees' ability to acquire water, thereby affecting the overall transpiration rate. Research has shown that moderate stand density can optimize photosynthesis and the transpiration process, improving water use efficiency. On the other hand, excessively high density may lead to increased water stress, impacting tree growth and health (Tague et al., 2019). Keitel et al. (2003) showed for example a strong positive relationship between T and stem basal area in European beech stands. The subalpine region of Mount Gongga is characterized by highly frequent precipitation, resulting in a humid climate that provides ample water supply for plant transpiration.

Within the growing season, T was generally high in May, decreased in June, and reached high values again in July or August, followed by a continuous decrease to its minimum in October, which was generally consistent with previous studies (Wang et al., 2021; Wullschleger and Hanson, 2006; Xu et al., 2022). The decrease in transpiration in June might have been influenced by wind speed (Meinzer, 1993). The later peak in T in July and August was likely due to increased solar radiation,

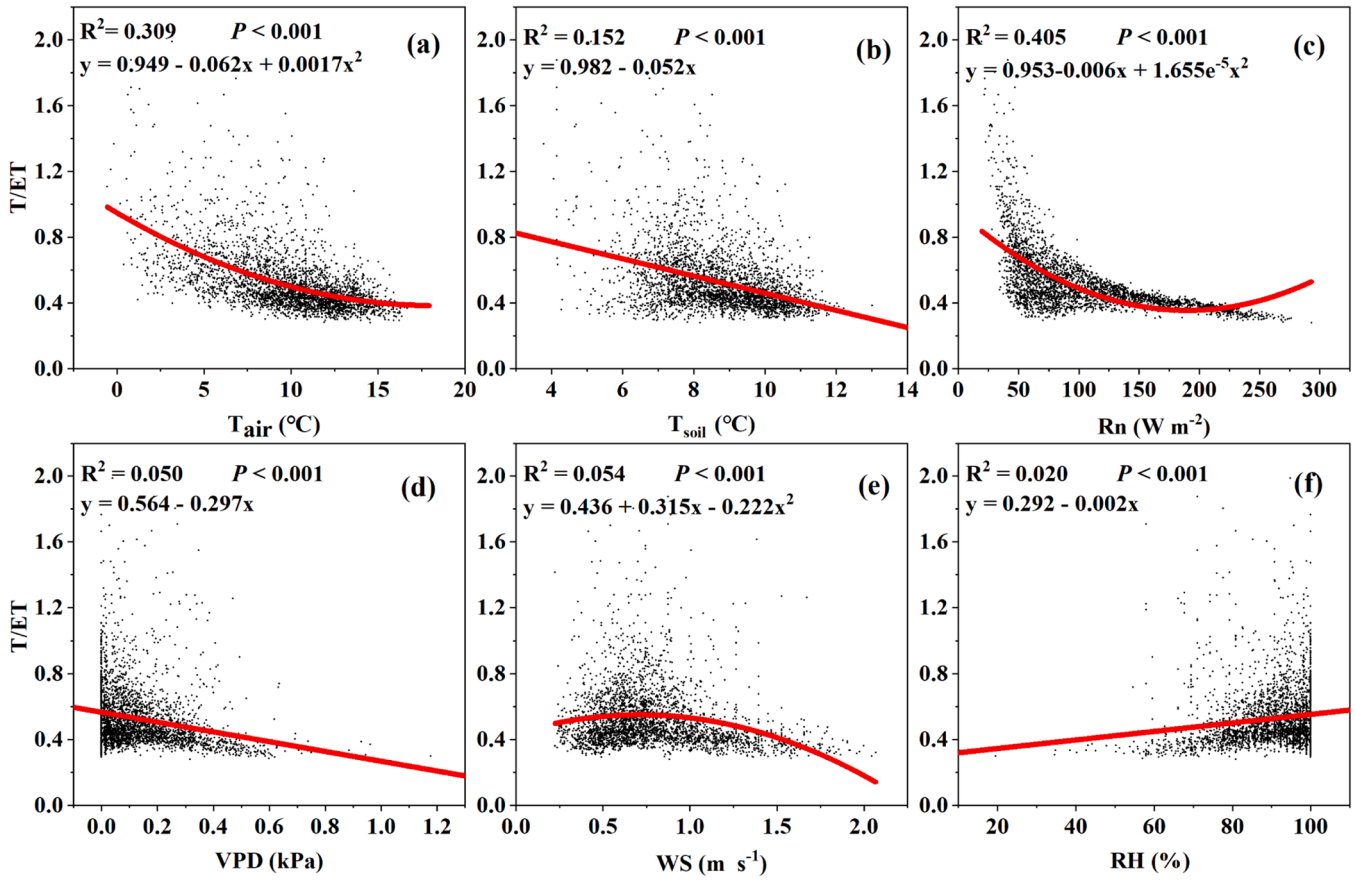

Fig. 8. The relationships between the daily ratio of transpiration to evapotranspiration (T/ET) with (a) air temperature (T_{air}, °C), (b) soil temperature (T_{soil}, °C), (c) net radiation (R_n, W m^{-2}), (d) vapor pressure deficit (VPD, kPa), (e) wind speed (Ws, m s^{-1}), and (f) relative humidity (RH, %).

higher T_{air}, and abundant P_{re} (Pei et al., 2022; Zhu et al., 2022). Towards September and October, radiation, P_{re} and T_{air} dropped, causing T to decrease. From 2005 to 2021, there was a slight decreasing trend in T, with an annual change rate of −2.46 mm $year^{-2}$ in present study. This decreasing trend was primarily influenced by VPD and temperature (Table 1). The decline in T may indicate a reduced water use efficiency of the forest during the growing season, which could impact plant growth and health. Due to changes in T/ET, future precipitation may manifest more as extreme events (such as heavy rainfall or drought), thereby affecting the availability and distribution of water resources and leading to changes in nearby ecosystems. The reduction in T and T/ET alters the dynamics of the water cycle, potentially resulting in decreased soil moisture and drier conditions, further impacting the health of terrestrial and aquatic ecosystems. This change may also increase surface runoff, affecting groundwater recharge and water resource availability (Schlesinger and Jasechko, 2014). However, the changing trends of T varied in different studies because of the discrepancies of the relationship between T and meteorological conditions across different sites (Hayat et al., 2022; Zhu et al., 2022). This can be attributed to the significant correlation between T and meteorological factors, which vary across different study sites.

T_{air}, T_{soil}, R_n, Ws, RH, and VPD had varying degrees of impact on T at different time scales (Table 1), which is consistent with the results of previous studies (Rawson et al., 1977; Wu et al., 2022; Zhu et al., 2022). R_n and VPD showed the highest correlation coefficients. At daily and monthly scales, R_n had the largest impact on T because the energy required for plant transpiration came from radiation (Mackova et al., 2014). Moreover, changes in R_n can also affect T_{air}, which in turn affected T. As the time scale expanded, the impact of VPD on T became increasingly significant and VPD was the strongest determinant for T at the annual scale. VPD as a proxy for the VPD difference between the water vapor saturated gaseous spaces within the leaves and the ambient atmosphere is the main driving force for water vapor diffusion through the stomata and, thus, affects water vapor transport in the canopy. When VPD changes, leaves also adjust their stomatal conductance to maintain the water balance in their tissues, also affecting T (Zhu et al., 2022). The influence of T_{air} and T_{soil} on T was relatively small. Temperature can affect leaf activity, causing changes in stomatal conductance and thus affecting plant T. However, for different regions, meteorological conditions and plant species, the response of T to meteorological factors also differs significantly: She et al. (2013) found through the study on T of *Caragana korshinskii* trees on an hourly scale that T increased exponentially with radiation, and decreased logarithmically with a decrease in VPD; Wu et al. (2022), however, reported that R_n had a negative effect on T, the effect of VPD on T was not significant on a daily scale, and the effects of various factors on T varied greatly in different hydrological years.

4.3. *Driving factors to the variations in T/ET during the growing season*

Zhu et al. (2015) conducted a study on three forest ecosystems in the Changbaishan temperate broad-leaved Korean pine mixed forest (CBS), the Qianyanzhou subtropical coniferous plantation (QYZ) and the Dinghushan subtropical evergreen mixed forest (DHS) in a north-south transect of eastern China. They quantified T/ET and found that the annual mean growing season T/ET ratio for three forests were 0.68 ± 0.07 (CBS), 0.64 ± 0.22 (QYZ) and 0.68 ± 0.11 (DHS), respectively. The PT-JPL model was also used to quantify multi-year average T/ET of different forest ecosystems in China, showing that T/ET ranged between 0.65 and 0.72 (Niu et al., 2019). Both these studies estimated higher

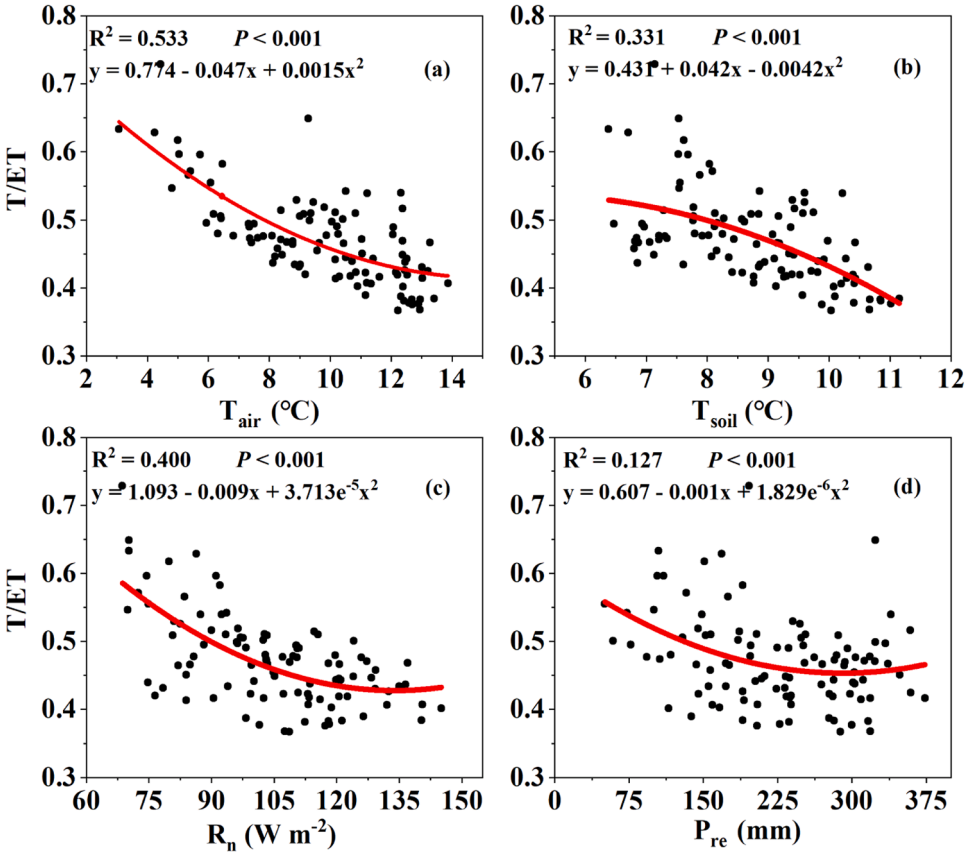

Fig. 9. The relationships between the monthly ratio of transpiration to evapotranspiration (T/ET) with (a) air temperature (T_{air}, °C), (b) soil temperature (T_{soil}, °C), (c) net radiation (R_n, W m^{-2}), and (d) precipitation (P_{re}, mm).

T/ET values than found in our study (0.46 ± 0.03). The subalpine area of Mount Gongga has high P_{re} and high ET with high forest density. Therefore, higher proportions of P_{re} (compared to the sites in the other studies) might intercepted and re-evaporated by the canopy, reducing T/ET (Tsiko et al., 2012; Hu et al., 2023). However, further research is needed to compare T/ET among different forest ecosystems and environmental boundary conditions.

There were differences in the relationship between T/ET of the subalpine coniferous forest and meteorological factors at different time scales, which is consistent with previous research (Pei et al., 2022). At the daily time scale, R_n had the most significant impact on T/ET whereas at the monthly time scale, the most significant meteorological factor affecting T/ET was T_{air}, followed by R_n. This result is consistent with findings of Petrik et al. (2022), who showed that T_{air} can explain about 50 % of the T/ET variation, as it may also capture the phenological development of leaves. However, they suggested that T_{air} was positively correlated with T/ET whereas our research showed a negative correlation (Ren et al., 2019). Our study found that meteorological factors (T_{air}, T_{soil}, P_{re}, R_n) affecting T/ET also had significant correlations with T and ET. Additionally, the effect of T_{air} on T was relatively small compared to that on ET, because other components of ET (soil evaporation and canopy interception) are usually more affected by T_{air} (Ventura et al., 2006; Zhou et al., 2018). In our humid subalpine forest (mean annual P_{re} >1800.00 mm, RH >80.00 %), ET is primarily energy-limited rather than water-limited due to sufficient water availability. Furthermore, ET exhibits higher sensitivity to R_n than T (Table 1 and S2), as canopy interception (E_i) is more responsive to meteorological variations (E_i contributes 25.50–31.30 % of ET) (Sun et al., 2013; Hu et al., 2023). The *Abies fabri* demonstrates conservative water-use strategies under persistently high humidity conditions, resulting in weaker responses of T to energy fluctuations compared to ET (Hu et al., 2023). Thus, when T_{air} changed, the change in ET was greater than that of T, leading to changes in T/ET and this was similar for Rn. However, Niu et al. (2019) found as Petrik et al. (2022) did that an increase in T_{air} led to higher T/ET. They postulated that both T and ET increase with rising T_{air}, but observed the correlation between T and T_{air} being stronger than that between ET and T_{air}. We might speculate that forest type might partially explain the observed differences. Petrik et al. (2022) for example report on a deciduous European beech forest, where leaf phenology (which has shown to be related to T_{air}) will have a stronger effect on T (but also on soil evaporation) as in our evergreen coniferous forest. Evergreen coniferous forests retain their leaves year-round, allowing them to continuously perform T throughout the entire growing season. Compared to deciduous forests that shed their leaves seasonally, the persistent leaf area of evergreen species helps maintain a more stable and potentially higher T/ET, resulting in a more consistent water use pattern. In contrast, deciduous forests experience higher T rates during the growing season but see a sharp decline during leaf senescence (Augusto et al., 2015).

P_{re} and T/ET were not significantly correlated at the daily and annual time scale but were significantly negatively correlated at the monthly time scale. The results of different previous studies on this point are not consistent. Zeppel et al. (2006) found that the relationship between P_{re} and ET became stronger at larger time scales. Zhu et al. (2015) assumed that interannual P_{re} had no significant effect on T/ET, while Niu et al. (2019) reported that P_{re} had a significant negative correlation with T/ET at annual time scale. When soil moisture is sufficient, plants can effectively transpire, promoting growth and photosynthesis, thereby maintaining the health of the ecosystem. However, when soil moisture is inadequate, plants are forced to adjust their water use strategies, such as closing their stomata to reduce water loss, which often leads to stunted growth and a decline in ecosystem productivity (Carminati et al., 2017). The replenishment of soil moisture in forested areas with different stand

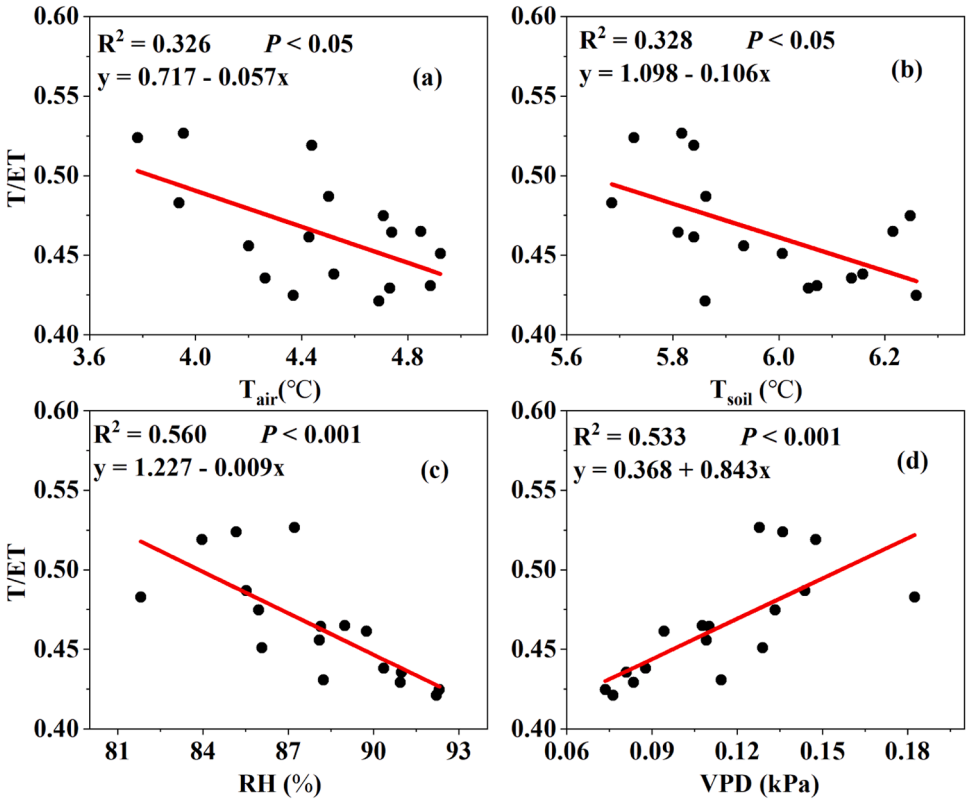

Fig. 10. The relationships between the annual ratio of transpiration to evapotranspiration (T/ET) with (a) air temperature (T_{air}, °C), (b) soil temperature (T_{soil}, °C), (c) relative humidity (RH, %), and vapor pressure deficit (VPD, kPa).

structures varies in response to P_{re}, thus explaining the observed differences in the impact on T (Raz-Yaseef et al., 2012). We also found that there were no significant differences in T/ET between different precipitation years. This was attributed to the abundant P_{re} at the study site, with even dry years receiving P_{re} exceeding 1400 mm, meaning the climate in the study site remained always moist. Some studies also found that the ET will remain constant or scattered when P_{re} exceeded a threshold (Hu et al., 2023; Igarashi et al., 2015; Zhang et al., 2001). Moreover, there was no significant difference of the VPD and RH among different precipitation years, which were the dominant drivers to the annual variations in T and T/ET (Fig. 10 and Table 1). The significant decline in T/ET after 2017 was mainly influenced by VPD and RH (Fig. 10). The decline in T/ET will lead to a reduction in water use efficiency, making plants more susceptible to water stress in arid conditions, while also impacting the health of ecosystems and biodiversity. This change may also reduce the carbon uptake capacity of plants, thereby affecting the global carbon cycle and providing feedback on local climate patterns. For agricultural and water resource managers, changes in T/ET will influence irrigation plans and water resource allocation, necessitating adjustments to meet the water demands of plants (Schlesinger and Jasechko, 2014).

It was mentioned earlier that plant phenology and moisture conditions can impact T/ET, but we may not have fully considered the impact of vegetation changes on the T/ET ratio and the role of soil moisture in the dynamics of T and ET in this study, mainly due to limitations in the scope of the research and conditions affecting data acquisition. Therefore, future research could focus on the impacts of vegetation changes and soil moisture on the evapotranspiration and its components.

5. Conclusions

In this study, three machine learning models (Random Forest, Support Vector Regression and Multi-layer Perceptron) were used to simulate the transpiration (T) of a subalpine coniferous forest in Mount Gongga, southwest China for the growing season from 2005 to 2021, and the ratios of T to the evapotranspiration (T/ET) were also computed for this period. Machine learning models performed better than the "traditional" Penman-Monteith model in simulating T. Although there was a slight overall decline in T and T/ET during 2005–2021, there was no significant changes in T/ET before 2016. T, ET and T/ET showed no significant difference among different precipitation years most likely due the high precipitation amount in this area. The dominant meteorological factor affecting T/ET varied among different time scales, with air temperature being most important at the daily, net radiation at the monthly, and relative humidity at the annual scale. From our results, it can be anticipated that in warming climate, the T/ET will continue to decrease, leading to reduced vegetation water use and increased runoff. This might, depending on other environmental conditions, lead to an increase in available water resources for agriculture and other human demand in the subalpine area but also increase the risk of flash floods.

CRediT authorship contribution statement

Yuhao Xiang: Writing – original draft, Methodology, Data curation. **Genxu Wang:** Writing – review & editing, Supervision. **Arthur Gessler:** Writing – review & editing, Conceptualization. **Xiangyang Sun:** Data curation. **Shan Lin:** Investigation. **Zishu Tang:** Data curation. **Shouqin Sun:** Funding acquisition. **Zhaoyong Hu:** Writing – review & editing, Supervision, Investigation, Conceptualization.

Declaration of competing interest

The authors declare that they have no known competing financial interests or personal relationships that could have appeared to influence the work reported in this paper.

Acknowledgements

This work was supported by the National Natural Science Foundation of China (42271063, 42330508, and 41901053), Science & Technology Fundamental Resources Investigation Program (2022FY100205) and the China Scholarship Council (201904910279). We also thank Gongga Mountain National Forest Ecosystem Research Station, Chinese Academy of Sciences, for their support for data collection.

Supplementary materials

Supplementary material associated with this article can be found, in the online version, at doi:10.1016/j.agrformet.2025.110692.

Data availability

Data will be made available on request.

References

Allawi, M.F., et al., 2023. Monthly rainfall forecasting modelling based on advanced machine learning methods: tropical region as case study. Eng. Appl. Comput. Fluid Mech. 17 (1), 550–564.
Allen, R.G., Pereira, L.S., Raes, D., Smith, M., 1998. Crop Evapotranspiration-Guidelines for Computing Crop Water Requirements-FAO Irrigation and Drainage Paper 56, 300. FAO, Rome, D05109.
Allen, R.G., Jensen, M.E., Wright, J.L., Burman, R.D., 1989. Operational estimates of reference evapotranspiration. Agron. J. 81 (4), 650–662.
Augusto, L., et al., 2015. Influences of evergreen gymnosperm and deciduous angiosperm tree species on the functioning of temperate and boreal forests. Biol. Rev. 90 (2), 444–466.
Arrieta, A.B., et al., 2020. Explainable artificial intelligence (XAI): concepts, taxonomies, opportunities and challenges toward responsible AI. Inf. Fusion 58, 82–115.
Bailey, B.J., et al., 1993. Transpiration of *ficusb enjamina* - comparison of measurements with predictions of the Penman-Monteith model and a simplified version. Agric. For. Meteorol. 65 (3–4), 229–243.
Benardos, P.G., Vosniakos, G.C., 2007. Optimizing feedforward artificial neural network architecture. Eng. Appl. Artif. Intell. 20 (3), 365–382.
Breiman, L., 2001. Random forests. Mach. Learn. 45 (1), 5–32.
Brutsaert, W., 2015. A generalized complementary principle with physical constraints for land-surface evaporation. Water Resour. Res. 51 (10), 8087–8093.
Carminati, A., et al., 2017. Root hairs enable high transpiration rates in drying soils. New Phytol. 216 (3), 771–781.
Cao, R.C., et al., 2020. Shifts in Ecosystem Water Use Efficiency On China's Loess Plateau Caused by the Interaction of Climatic and Biotic Factors Over 1985-2015, 291. Agricultural and Forest Meteorology, 108100.
Chang, C.C., Lin, C.J., 2011. LIBSVM: a library for support vector machines. ACM Trans. Intell. Syst. Technol. 2 (3), 27.
Chen, Z.H., Chi, Z.R., Fu, H., Feng, D.G., 2013. Multi-instance multi-label image classification: a neural approach. Neurocomputing 99, 298–306.
Cheng, Y.G., Brutsaert, W., 2005. Flux-profile relationships for wind speed and temperature in the stable atmospheric boundary layer. Boundary Layer Meteorol. 114 (3), 519–538.
Cortes, C., Vapnik, V., 1995. Support-vector networks. Mach. Learn. 20 (3), 273–297.
Dong, S., Wang, P., Abbas, K., 2021. A survey on deep learning and its applications. Comput. Sci. Rev. 40, 100379.
Ellsasser, F., et al., 2020. Predicting tree sap flux and stomatal conductance from drone-recorded surface temperatures in a mixed agroforestry system-a machine learning approach. Remote Sens (Basel) 12 (24), 4070.
Fatichi, S., Pappas, C., 2017. Constrained variability of modeled *T/ET* ratio across biomes. Geophys. Res. Lett. 44 (13), 6795–6803.
Fan, J., Lu, X., 2010. Plant biomass and nutrient accumulation in subalpine dark coniferous forest of Gongga mountain, Southwest China. In: Proceedings 2010 International Conference on Challenges in Environmental Science and Computer Engineering (CESCE 2010), pp. 63–68.
Gocic, M., et al., 2016. Long-term precipitation analysis and estimation of precipitation concentration index using three support vector machine methods. Adv. Meteorol., 7912357, 2016.
Granier, A., Huc, R., Barigah, S.T., 1996. Transpiration of natural rain forest and its dependence on climatic factors. Agric. For. Meteorol. 78 (1–2), 19–29.
Gu, C.J., et al., 2018. Partitioning evapotranspiration using an optimized satellite-based et model across biomes. Agric. For. Meteorol. 259, 355–363.
Han, X., et al., 2023. The effect of time scales on the distribution of evapotranspiration and driving factors in desert grasslands. Agric. Water Manage. 284, 108348.
Hatton, T.J., Catchpole, E.A., Vertessy, R.A., 1990. Integration of sapflow velocity to estimate plant water use. Tree Physiol. 6 (2), 201–209.
Hayat, M., et al., 2022. Environmental Control on Transpiration and Its Cooling Effect of *Ficus Concinna* in a Subtropical City Shenzhen, Southern China, 312. Agricultural and Forest Meteorology, 108715.
Hou, P.P., et al., 2023. Transpiration characteristics and environmental controls of orange orchards in the dry-hot valley region of southwest China. Agric. Water Manage. 288, 108467.
Hu, Z.Y., et al., 2023. Controlling factors of the spatial-temporal fluctuations in evapotranspiration along an elevation gradient across humid montane ecosystems. Water Resour. Res. 59 (1) e2022WR033228.
Hu, Z.Y., et al., 2018. Spatial-temporal patterns of evapotranspiration along an elevation gradient on Mount Gongga, southwest China. Water Resour. Res. 54 (6), 4180–4192.
Igarashi, Y., et al., 2015. Separating physical and biological controls on long-term evapotranspiration fluctuations in a tropical deciduous forest subjected to monsoonal rainfall. J. Geophys. Res.-Biogeosci. 120 (7), 1262–1278.
Jasechko, S., et al., 2013. Terrestrial water fluxes dominated by transpiration. Nature 496 (7445), 347–350.
Jiménez-Rodríguez, C.D., Sulis, M., Schymanski, S., 2024. The role of the intraspecific variability of hydraulic traits for modeling the plant water use in different european forest ecosystems. J. Adv. Model. Earth Syst. 16 (3) e2022MS003494.
Jordan, M.I., Mitchell, T.M., 2015. Machine learning: trends, perspectives, and prospects. Science 349 (6245), 255–260.
Jump, A.S., et al., 2017. Structural overshoot of tree growth with climate variability and the global spectrum of drought-induced forest dieback. Glob. Chang. Biol. 23 (9), 3742–3757.
Kassanuk, T., Phasinam, K., 2022. Impact of internet of things and machine learning in smart agriculture. ECS Trans. 107 (1), 3215–3222.
Keitel, C., Adams, M., Holst, T., Matzarakis, A., Mayer, H., Rennenberg, H., Gessler, A., 2003. Carbon and oxygen isotope composition of organic compounds in the phloem sap provides a short-term measure for stomatal conductance of European beech (*Fagus sylvatica* L.). Plant. Cell Environ., 26, 1157–1168.
LeCun, Y., Bengio, Y., Hinton, G., 2015. Deep learning. Nature 521 (7553), 436–444.
Lian, X.Et al., 2018. Partitioning global land evapotranspiration using CMIP5 models constrained by observations. Nat. Clim. Chang. 8 (7), 640–646.
Liang, W., Chen, Y., Fang, G., Kaldybayev, A., 2023. Machine learning method is an alternative for the hydrological model in an alpine catchment in the Tianshan region, central Asia. J. Hydrol.: Regional Studies 49, 101492.
Loescher, H.W., Gholz, H.L., Jacobs, J.M., Oberbauer, S.F., 2005. Energy dynamics and modeled evapotranspiration from a wet tropical forest in Costa Rica. J. Hydrol. 315 (1–4), 274–294.
Mackova, L., et al., 2014. Analysis of the impact of meteorological characteristics on the transpiration simulated in SIBYLA growth simulator. In: International Conference on Mendel and Bioclimatology. Brno, CZECH REPUBLIC, pp. 204–209.
Meinzer, F.C., 1993. Stomatal control of transpiration. Trends Ecol. Evol. (Amst.) 8 (8), 289–294.
Monteith, J.L., 1965. Evaporation and environment. Symp. Soc. Exp. Biol. 19, 205–234.
Murdiyarso, D., et al., 2015. The potential of Indonesian mangrove forests for global climate change mitigation. Nat. Clim. Chang. 5 (12), 1089–1092.
Niu, Z.G., et al., 2019. An Increasing Trend in the Ratio of Transpiration to Total Terrestrial Evapotranspiration in China from 1982 to 2015 Caused by Greening and Warming, 279. Agricultural and Forest Meteorology, 107701.
Paschalis, A., Fatichi, S., Pappas, C., Or, D., 2018. Covariation of vegetation and climate constrains present and future t/et variability. Environ. Res. Lett. 13 (10), 104012.
Pei, D.J., et al., 2022. Path Analysis of the Main Control Factors of Transpiration in greenhouse, Drip-Irrigated Grapes in Cold Areas of Northeast China, 14. Water, p. 3764.
Penman, H.L., 1948. Natural evaporation from open water, bare soil and grass. Proceed. Royal Society London Series a-Math. Phys. Sci. 193 (1032), 120–145.
Petrik, P., et al., 2022. Impact of Environmental Conditions and Seasonality on Ecosystem Transpiration and Evapotranspiration Partitioning (T/ET ratio) of Pure European Beech Forest, 14. Water, p. 3015.
Pnevmatikos, J.D., Katsoulis, B.D., 2006. The changing rainfall regime in Greece and its impact on climatological means. Meteorol. Appl. 13 (4), 331–345.
Priestley, C.H.B., Taylor, R.J., 1972. Assessment of surface heat-flux and evaporation using large-scale parameters. Mon. Weather Rev. 100 (2), 81–92.
Rawson, H.M., Begg, J.E., Woodward, R.G., 1977. Effect of atmospheric humidity on photosynthesis, transpiration and water-use efficiency of leaves of several plant species. Planta 134 (1), 5–10.
Raz-Yaseef, N., Yakir, D., Schiller, G., Cohen, S., 2012. Dynamics of evapotranspiration partitioning in a semi-arid forest as affected by temporal rainfall patterns. Agric. For. Meteorol. 157, 77–85.
Ren, X.L., Lu, Q.Q., He, H.L., Zhang, L., Niu, Z.E., 2019. Estimation and analysis of the ratio of transpiration to evapotranspiration in forest ecosystems along the north-south transect of east China. J. Geog. Sci. 29 (11), 1807–1822.
Schlesinger, W.H., Jasechko, S., 2014. Transpiration in the global water cycle. Agric. For. Meteorol. 189, 115–117.
Schmidhuber, J., 2015. Deep learning in neural networks: an overview. Neural. Netw. 61, 85–117.
She, D.L., Xia, Y.Q., Shao, M.A., Peng, S.Z., Yu, S.G., 2013. Transpiration and canopy conductance of *Caragana korshinskii* trees in response to soil moisture in sand land of China. Agroforestry Systems 87 (3), 667–678.
Sperling, O., Yermiyahu, U., Hochberg, U., 2023. Linking almond trees' transpiration to irrigation's mineral composition by physiological indices and machine learning. Irrigat. Sci. 41 (4), 487–499.
Sun, J.Y., Sun, X.Y., Hu, Z.Y., Wang, G.X., 2020. Exploring the influence of environmental factors in partitioning evapotranspiration along an elevation gradient on Mount Gongga, eastern edge of the Qinghai Tibet Platea, China. J. Mountain Sci. 17 (2), 384–396.

Sun, X.Y., Wang, G.X., Lin, Y., Liu, L.N., Gao, Y., 2013. Intercepted rainfall in *abies fabri* forest with different-aged stands in southwestern China. Turk. J. Agric. For. 37 (4), 495–504.
Tague, C.L., Moritz, M., Hanan, E., 2019. The Changing Water Cycle: The Eco-Hydrologic Impacts of Forest Density Reduction in Mediterranean (seasonally dry) Regions, 6. Wiley Interdisciplinary Reviews-Water, p. e1350.
Tang, Z.S., et al., 2023. Elevational variations in stem hydraulic efficiency and safety of *Abies fabri*. Funct. Ecol. 37 (10), 2570–2582.
Tang, Z.S., Wang, G.X., Hu, Z.Y., 2022. Characteristics of stem sap flow and influencing factors of *Abies fabri* in varied diameters on Mount Gongga, China. Mountain Res. 40 (2), 220–234 in Chinese with English abstract.
Theil, H., 1950. A rank-invariant method of linear and polynomial regression analysis. Indagat. Math. 12 (85), 173.
Tsiko, C.T., Makurira, H., Gerrits, A.M.J., Savenije, H.H.G., 2012. Measuring forest floor and canopy interception in a savannah ecosystem. Phys. Chem. Earth 47-48, 122–127.
Ventura, F., Snyder, R.L., Bali, K.M., 2006. Estimating evaporation from bare soil using soil moisture data. J. Irrig. Drain. Eng. 132 (2), 153–158.
Wang, L., et al., 2021. Estimate canopy transpiration in larch plantations via the interactions among reference evapotranspiration, leaf area index, and soil moisture. For. Ecol. Manage. 481, 118749.
Wang, W., Jia, M., Wang, G., Zhu, W., McDowell, N.G., 2017. Rapid warming forces contrasting growth trends of subalpine fir (*Abies fabri*) at higher- and lower-elevations in the eastern Tibetan Plateau. For. Ecol. Manage. 402, 135–144.
Wei, Z.W., et al., 2017. Revisiting the contribution of transpiration to global terrestrial evapotranspiration. Geophys. Res. Lett. 44 (6), 2792–2801.
Wu, Y.H., Li, W., Zhou, J., Cao, Y., 2013. Temperature and precipitation variations at two meteorological stations on eastern slope of Gongga Mountain, SW China in the past two decades. J. Mt. Sci. 10 (3), 370–377.
Wu, Y.H., et al., 2022. Environmental factors driving the transpiration of a *Betula platyphylla sukaczev* forest in a semi-arid region in north China during different hydrological years. Forests 13 (10), 1729.
Wullschleger, S.D., Hanson, P.J., 2006. Sensitivity of canopy transpiration to altered precipitation in an upland oak forest: evidence from a long-term field manipulation study. Glob. Chang. Biol. 12 (1), 97–109.
Xiao, J.F., et al., 2013. Carbon fluxes, evapotranspiration, and water use efficiency of terrestrial ecosystems in China. Agric. For. Meteorol. 182, 76–90.
Xu, Z.P., Man, X.L., Cai, T.J., Shang, Y.X., 2022. How potential evapotranspiration regulates the response of canopy transpiration to soil moisture and leaf area index of the boreal larch forest in China. Forests 13 (4), 571.
Zhan, M.Y., et al., 2022. Impacts of vegetation changes on land evapotranspiration in China during 1982-2015. Front. Environ. Sci. 10, 819277.
Zhang, L., Dawes, W.R., Walker, G.R., 2001. Response of mean annual evapotranspiration to vegetation changes at catchment scale. Water Resour. Res. 37 (3), 701–708.
Zeppel, M.J.B., Yunusa, I.A.M., Eamus, D., 2006. Daily, seasonal and annual patterns of transpiration from a stand of remnant vegetation dominated by a coniferous *Callitris* species and a broad-leaved eucalyptus species. Physiol. Plant. 127 (3), 413–422.
Zhou, S., Yu, B.F., Zhang, Y., Huang, Y.F., Wang, G.Q., 2018. Water use efficiency and evapotranspiration partitioning for three typical ecosystems in the Heihe River Basin, northwestern China. Agric. For. Meteorol. 253, 261–273.
Zhou, S., Yu, B.F., Zhang, Y., Huang, Y.F., Wang, G.Q., 2016. Partitioning evapotranspiration based on the concept of underlying water use efficiency. Water Resour. Res. 52 (2), 1160–1175.
Zhou, P., 2013. The Differentiation and Influence Factors of Carbon Sequestration of Typical Vegetation Types in Altitudinal Belts of Gongga Mountain. Master dissertation. Institute of Mountain Hazards and Environment, Chinese Academy of Sciences.. Chinese with English abstract.
Zhu, X.J., et al., 2015. Spatiotemporal variations of T/ET (the ratio of transpiration to evapotranspiration) in three forests of eastern China. Ecol. Indic. 52, 411–421.
Zhu, Y., et al., 2022. Influencing factors for transpiration rate: a numerical simulation of an individual leaf system. Thermal Sci. Eng. Progress 27, 101110.